

Parallel Split Learning with Global Sampling

Mohammad Kohankhaki¹, Ahmad Ayad², Mahdi Barhoush³ and Anke Schmeink⁴

Abstract—The expansion of IoT devices and the demands of Deep Learning have highlighted significant challenges in Distributed Deep Learning (DDL) systems. Parallel Split Learning (PSL) has emerged as a promising derivative of Split Learning that is well suited for distributed learning on resource-constrained devices. However, PSL faces several obstacles, such as large effective batch sizes, non-IID data distributions, and the straggler effect. We view these issues as a sampling dilemma and propose to address them by orchestrating the mini-batch sampling process on the server side. We introduce the Uniform Global Sampling (UGS) method to decouple the effective batch size from the number of clients and reduce mini-batch deviation in non-IID settings. To address the straggler effect, we introduce the Latent Dirichlet Sampling (LDS) method, which generalizes UGS to balance the trade-off between batch deviation and training time. Our simulations reveal that our proposed methods enhance model accuracy by up to 34.1% in non-IID settings and reduce the training time in the presence of stragglers by up to 62%. In particular, LDS effectively mitigates the straggler effect without compromising model accuracy or adding significant computational overhead compared to UGS. Our results demonstrate the potential of our methods as a promising solution for DDL in real applications.

Index Terms—Parallel split learning, distributed deep learning, latent dirichlet sampling, uniform global sampling.

I. INTRODUCTION

RECENT advances in Deep Learning (DL), driven by growing architecture sizes, have significantly impacted areas like audio signal processing, natural language processing, and smart healthcare [1]–[5]. This progress relies on large data volumes and substantial computing resources [6]–[8]. The expansion of Internet-of-Things (IoT) devices, such as smartphones and wearables, provides extensive data and computing capabilities, yet privacy laws often restrict access to this data [6]. Distributed Deep Learning (DDL) frameworks have emerged to address these challenges by enabling collaborative model training across multiple devices while preserving data privacy.

Federated Learning (FL) [9] is a prominent framework in DDL. In Federated Averaging (FedAvg), clients train model copies locally and periodically aggregate these models by averaging their parameters, facilitating global model convergence [9]. However, the high resource demands of FL restrict its implementation in edge computing and IoT environments, primarily due to substantial computational and communication burdens. Deploying FL on edge devices is further complicated by the straggler effect [10], which causes significant delays.

Additionally, FL struggles with datasets that are small or non-independent and identically distributed (non-IID). Strategies such as client selection [11] and model quantization [12] help mitigate these issues, but do not resolve them completely.

Split Learning (SL) [13], [14] addresses some limitations of FL by partitioning neural network training between client devices and a central server. Clients conduct initial Forward Propagation (FP) on local data and send intermediate results to the server, which completes the FP, initiates the Backward Propagation (BP) and returns gradients to the clients to complete the BP. SL enhances data privacy, reduces computational demands on the client-side, and increases the convergence speed compared to FL, making it well-suited for edge and IoT applications [13], [15], [16]. However, it incurs high training and communication latency due to its sequential nature [15]. While SL performs better than FL with non-IID data [16], [17], it suffers from catastrophic forgetting as the number of clients increases [18].

To address training latency in SL, advanced derivatives of SL like Split Federated Learning (SFL) [19]–[21] and Parallel Split Learning (PSL) [22]–[26] have been proposed. SFL combines the techniques of SL and FL to facilitate parallel model training across multiple devices. This approach leverages the advantages of both FL and SL. However, it encounters increased communication overhead compared to SL because it requires both the transmission of intermediate model results from clients to the server and the aggregation of updated models back to clients. Furthermore, SFL necessitates that the server maintains individual model copies for each client, which complicates scalability. Although variants such as SFLv2, SFLv3 [20], and SFLG [21] aim to mitigate these drawbacks, practical challenges persist.

PSL enhances parallelism without requiring multiple server model instances or client model aggregation. However, PSL still faces issues with large effective batch sizes, non-IID data, and the straggler effect:

- 1) **Large Effective Batch Size Problem** [27]: Also known as the *Server-Client Update Imbalance Problem* [25], where the effective batch size scales with the number of clients.
- 2) **Non-Independent and Identically Distributed Data**: Devices contribute data of varying distributions and sizes, causing batch distributions to deviate from the overall data distribution and leading to poor generalization.
- 3) **Straggler Effect**: Due to the need for synchronization, slower devices delay the training process, as the processing time of a single batch is determined by the slowest client, impacting throughput and total training time [10].

All authors are with the Chair of Information Theory and Data Analytics, RWTH Aachen University, D-52074 Aachen, Germany. E-Mails^{1,2,3,4}: {mohammad.kohankhaki, ahmad.ayad, mahdi.barhoush, anke.schmeink}@inda.rwth-aachen.de

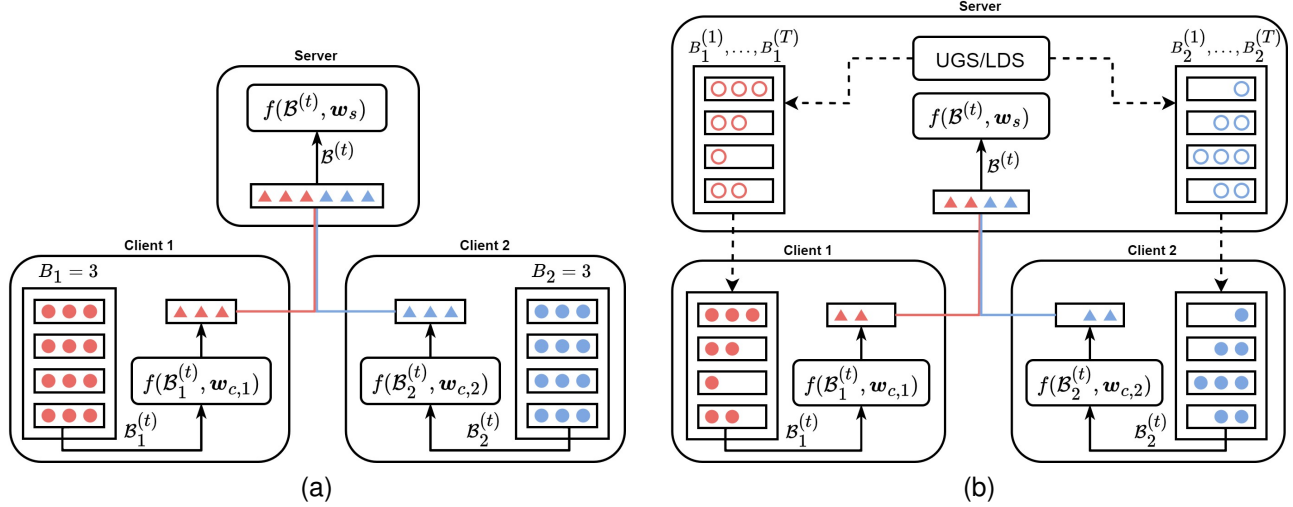


Fig. 1. A schematic illustration of sampling local batch sizes with fixed (a) and variable (b) local batch sizes. The proposed UGS and LDS methods allow for variable local batch sizes that sum up to a fixed global batch size, which enables fine-grained control over the sampling process. This flexibility is crucial for mitigating the challenges of large effective batch sizes, non-IID data, and the straggler effect in PSL.

We propose the Uniform Global Sampling (UGS) method as an extension of the PSL framework introduced in [22] to address the problems (1) and (2). UGS addresses problem (1) by allowing for variable local batch sizes that sum up to a fixed global size. This decouples the number of clients from the effective batch size. By analysing the deviation probability of global batches¹ from the overall data distribution, we show that the choice of the local batch sizes is crucial for the model convergence. In particular, we show that using fixed local batch sizes can increase the deviation probability of the global batches, especially in the presence of non-IID data. In UGS, the local batch sizes are sampled according to client selection probabilities. We show that if the client selection probabilities are proportional to the dataset sizes, the deviation bound of the global batches is at least as tight as for uniform sampling in central learning.

Inspired by the Latent Dirichlet Allocation model [28], we introduce the Latent Dirichlet Sampling (LDS) method as a generalization of UGS to address the straggler effect (3). LDS introduces a Dirichlet prior distribution over the client selection probabilities to control the incidence of stragglers in batches. The prior distribution is adjusted based on the delay times of the straggler clients and a trade-off hyperparameter. The client selection probabilities are estimated using the Expectation-Maximization (EM) algorithm for Maximum A Posteriori (MAP) estimation [29]. LDS balances the trade-off between batch deviation and training time by sampling local batch sizes according to these estimated client selection probabilities.

An overview of our methods is shown in Figure 1. Extensive simulation results demonstrate that the proposed UGS and LDS methods can significantly improve the accuracy and convergence speed of PSL, especially in the presence of non-IID data. Our results show that LDS effectively mitigates

the straggler effect without compromising the model accuracy or adding significant computational overhead compared to UGS.

Contributions & Organization

- We analyse the deviation probability of global batches in PSL and show why the choice of the local batch size is crucial for the convergence of the model (Section IV-A).
- We introduce the UGS method to address the large effective batch size problem and the non-IID data problem in PSL (Section IV-B).
- Motivated by the straggler effect problem, we introduce LDS to balance the trade-off between batch deviation and training time, ensuring efficient and accurate model training (Section IV-C).

Our code and all the results of this work are publicly available on GitHub [30].

II. RELATED WORK

PSL enables the parallel execution of the FP and BP on the clients and enhances scalability by avoiding the need for the server to maintain separate model copies for each client. Nevertheless, PSL faces the client decoupling problem [27] (also known as client detachment problem [25]), where the information flow between clients is decoupled during the BP due to the independent execution of the BP on each client. Jeon and Kim [22] use gradient averaging over all clients to address the client decoupling problem. They chose the local batch sizes fixed and proportional to the dataset size of each client. Lyu et al. [31] propose averaging the clients' local loss function outputs instead of their local gradients. This approach aligns with that of [22] due to the linearity of the gradient operator, but enhances privacy as clients can compute the local loss functions without sharing labels. [22] and [31] show consistent convergence and improved accuracy in both IID and

¹We use the term *batch* to refer to mini-batches in the context of DL. The difference between global and local batches is explained in Section III.

non-IID settings, but do not address the large effective batch size problem.

Pal et al. [27] propose SplitAvg to address the client decoupling problem. This method generalizes the approach in [22] by allowing averaging only a subset of the local gradients. Opposed to [22] and [31], the authors observe that using all clients for gradient averaging, the model may not converge. To address the large effective batch size problem, the authors propose scaling the learning rate on the server side while keeping the local batch size fixed and identical for all clients. Following the line of work from [26], Oh et al. [25] propose using smashed data augmentation, local loss function design and FedAvg for the client models to overcome the large effective batch size problem and client model decoupling.

[27] and [25] provide promising solutions for the large effective batch size problem, but assume that the effective batch size scales with the number of clients. This assumption conflicts with the diminishing returns of larger batch sizes for gradient estimation [32] and the benefits of smaller batch sizes [33]. Furthermore, the empirical results are reported only for IID settings. They do not address the non-IID data problem, which is a significant challenge in PSL. For general SL, Cai and Wei [34] propose a method to handle non-IID data with a distillation loss function. The bargaining game approach for personalized SL [35] balances energy consumption and privacy in non-IID settings. However, these methods can not be directly applied to PSL.

Other efforts to improve PSL focus on reducing training and communication latency [23], [24], [36]. Methods include last-layer gradient aggregation, resource optimization, client clustering and cut-layer selection. However, these methods do not address the straggler effect, which remains a significant challenge in PSL. A notable work in this direction is the BOA algorithm [37], which dynamically adjusts the batch size of slow clients in distributed learning systems to reduce the straggler effect.

Different from other works, we approach the large effective batch size problem, the Non-IID data problem and the straggler effect as a sampling dilemma. By orchestrating the batch sampling process on the server side we allow variable local batch sizes and decouple the number of clients from the effective batch size. This enables global sampling methods to account for Non-IID data by reducing the deviation between the global batches and the overall data distribution and to mitigate the straggler effect by controlling the concentration of stragglers in global batches.

III. PRELIMINARIES

We consider the PSL setting from [22] where a server and $K \in \mathbb{N}$ clients train a neural network model with parameter vector \mathbf{w} collaboratively using the PSL framework. The set of clients is represented by $\mathcal{K} = \{1, 2, \dots, K\}$. We focus on supervised classification tasks, where the dataset \mathcal{D}_k of each client $k \in \mathcal{K}$ consists of input-label pairs $\mathcal{D}_k = \{(\mathbf{x}_{k,i}, y_{k,i})\}_{i=1}^{D_k}$, where $D_k \in \mathbb{N}$ is the dataset size, $\mathbf{x}_{k,i}$ is the input data, and $y_{k,i} \in \mathcal{M}$ is the ground truth class label of $\mathbf{x}_{k,i}$. Here, $\mathcal{M} = \{1, 2, \dots, M\}$ represents all classes

and $M \in \mathbb{N}$ is the number of classes. The overall dataset $\mathcal{D}_0 = \bigcup_{k=1}^K \mathcal{D}_k$ is the union of all clients' datasets, with a total size $D_0 = \sum_{k=1}^K D_k$. We refer to the distribution of the datapoints in \mathcal{D}_0 as the *empirical distribution*. We define the class counting function $c : \mathbb{N}^N \times \mathbb{N} \rightarrow \mathbb{N}$ with $N \in \mathbb{N}$ as

$$c(\mathbf{y}, m) = \sum_{i=1}^N \delta(y_i, m)$$

$$\text{where } \delta(i, j) = \begin{cases} 1 & \text{if } i = j \\ 0 & \text{otherwise} \end{cases}$$

The class distribution of a client k with class label vector $\mathbf{y}_k \in \mathcal{M}^{D_k}$ is denoted as $\beta_k \in \mathbb{R}^M$ with $\beta_k = \frac{1}{D_k}(c(\mathbf{y}_k, 1), c(\mathbf{y}_k, 2), \dots, c(\mathbf{y}_k, M))^T$. The *overall class distribution* of \mathcal{D}_0 with class label vector $\mathbf{y}_0 \in \mathcal{M}^{D_0}$ is denoted as $\beta_0 \in \mathbb{R}^M$ according to the same definition.

Every epoch consists of $T \in \mathbb{N}$ optimization steps. The set of optimization steps is denoted as $\mathcal{T} = \{1, 2, \dots, T\}$. We use the subscript k for clients and the superscript t for optimization steps. If the distinction is unnecessary, we omit the indices for brevity. Each client has a local batch size $B_k \in \mathbb{N}$. The global batch size $B = \sum_{k=1}^K B_k$ is the total number of data points that arrive at the server in each optimization step. Accordingly, we differentiate between local batches $\mathcal{B}_k^{(t)} \subseteq \mathcal{D}_k$ and the global batch $\mathcal{B}^{(t)} = \bigcup_{k=1}^K \mathcal{B}_k^{(t)}$ in each optimization step.

PSL mirrors SL by splitting the model parameters into a client-side lower segment \mathbf{w}_c and a server-side upper segment \mathbf{w}_s with $\mathbf{w} = (\mathbf{w}_s, \mathbf{w}_c)^T$. The first layer on the server side is referred to as the *cut layer*. Before training, the server sends \mathbf{w}_c to the clients, each storing a copy $\mathbf{w}_{c,k}$ with identical initial values. The function $f(\mathbf{x}; \mathbf{w})$ maps \mathbf{x} to a predicted value according to the given model parameters \mathbf{w} . Hence, the global model is given as $f(\mathbf{x}; \mathbf{w}) = f(f(\mathbf{x}; \mathbf{w}_c); \mathbf{w}_s)$. When the argument of f is a dataset or a subset of it, e.g. a batch \mathcal{B} with batch size B , it operates element-wise on the input data and is defined as:

$$f(\mathcal{B}; \mathbf{w}) = \{(f(\mathbf{x}_i; \mathbf{w}), y_i)\}_{i=1}^B$$

The goal is to find the optimal model parameters $\mathbf{w}^* = (\mathbf{w}_s^*, \mathbf{w}_c^*)^T$ that minimize the global loss function $L(\mathcal{D}_0; \mathbf{w})$:

$$\begin{aligned} \mathbf{w}^* &= \arg \min_{\mathbf{w}} L(\mathcal{D}_0; \mathbf{w}) \\ &= \arg \min_{\mathbf{w}} \frac{1}{D_0} \sum_{k=1}^K \sum_{i=1}^{D_k} L((\mathbf{x}_{k,i}, y_{k,i}); \mathbf{w}) \\ &= \arg \min_{\mathbf{w}} \frac{1}{D_0} \sum_{k=1}^K \sum_{i=1}^{D_k} L((f(\mathbf{x}_{k,i}; \mathbf{w}_c), y_{k,i}); \mathbf{w}_s) \end{aligned}$$

The mini-batch Stochastic Gradient Descent (SGD) algorithm or one of its variants are typically used to optimize the model parameters, alternating between FP and BP. Each optimization step $t \in \mathcal{T}$ involves the following substeps.

1) Parallel Client-Side FP

Each client k samples a local batch $\mathcal{B}_k^{(t)} \subseteq \mathcal{D}_k$ with a local batch size of B_k uniformly at random without replacement and sends $f(\mathcal{B}_k^{(t)}; \mathbf{w}_c)$ to the server.

2) Server-Side FP

Upon receiving all intermediate results from the clients, the server concatenates them to obtain the global batch $\mathcal{B}^{(t)} = \bigcup_{k=1}^K f(\mathcal{B}_k^{(t)}; \mathbf{w}_c)$. The server then computes the final prediction-label pairs $f(\mathcal{B}^{(t)}; \mathbf{w}_s)$ to calculate the average loss $L(\mathcal{B}^{(t)}; \mathbf{w}_s)$.

3) Server-Side BP

The server computes the gradient $\mathbf{g}_{\mathbf{w}_s}^{(t)} = \nabla_{\mathbf{w}_s} L(\mathcal{B}^{(t)}; \mathbf{w}_s)$. Using the learning rate $\eta \in \mathbb{R}$, the server updates its model parameters to $\mathbf{w}_s^{(t+1)} = \mathbf{w}_s^{(t)} - \eta \mathbf{g}_{\mathbf{w}_s}^{(t)}$. The server then broadcasts the gradient of the cut layer to all clients.

4) Parallel Client-Side BP

Upon receiving the cut layer gradient, each client k computes the gradient $\mathbf{g}_{\mathbf{w}_{c,k}}^{(t)} = \nabla_{\mathbf{w}_c} L(\mathcal{B}^{(t)}; \mathbf{w}_s)$ and sends it back to the server.

5) Server-Side Gradient Averaging

Upon receiving all gradients from the clients, the server computes the average client gradient $\bar{\mathbf{g}}_{\mathbf{w}_c}^{(t)} = \sum_{k=1}^K \frac{D_k}{D_0} \mathbf{g}_{\mathbf{w}_{c,k}}^{(t)}$ and broadcasts it to all clients.

6) Parallel Client-Side Model Update

Each client k uses $\bar{\mathbf{g}}_{\mathbf{w}_c}^{(t)}$ to update its model parameters $\mathbf{w}_{c,k}^{(t+1)} = \mathbf{w}_{c,k}^{(t)} - \eta \bar{\mathbf{g}}_{\mathbf{w}_c}^{(t)}$, using the same learning rate η as the server.

An epoch is concluded after T optimization steps. T is determined by the number of non-empty global batches that can be formed from the clients' datasets until depletion. The model is trained for a fixed number of epochs $E \in \mathbb{N}$. Note that since the client models are initialized with the same parameters \mathbf{w}_c and are always updated with the same gradients $\bar{\mathbf{g}}_{\mathbf{w}_c}^{(t)}$, they remain identical throughout the training process.

We make the following simplifying assumptions throughout this work:

Availability of Client Classes and Dataset Sizes: The server has access to the class counts and dataset sizes of all clients. It is important to note that in all SL-based frameworks, the class labels are shared during training and can be easily collected by the server. Therefore, providing the class counts or dataset sizes to the server does not introduce additional privacy concerns. The class distributions can be inferred from the class counts and dataset sizes.

Multinomial Approximation of Uniform Sampling: We model the distribution of local batches that are sampled uniformly at random without replacement as a multinomial

distribution. The correct model would be a hypergeometric distribution. However, assuming that usually $B_k \ll D_k$, the multinomial distribution closely approximates the hypergeometric distribution.

Stable Per-Epoch Delay Times: We assume that the delay times of the straggler clients do not change significantly during an epoch. The server keeps an updated estimate of the delay times $\omega_k \in \mathbb{R}_{\geq 0}$ for each client k . We define the delay time of a client as the difference between the processing time of the client and the processing time of the fastest client. The delay times are always relative to the fastest client, i.e., the fastest client k' has a delay time of $\omega_{k'} = 0$. The server may initially set the delay times to zero, if no prior knowledge is available

A summary of notations used in this work can be found in Table I.

TABLE I
SUMMARY OF NOTATIONS.

Notation	Description
\mathcal{K}	Index set for the K clients.
\mathcal{D}_k	Dataset of client k . $k = 0$ for overall dataset.
D_k	Dataset size of dataset \mathcal{D}_k . $k = 0$ for overall dataset.
\mathcal{M}	Set of all M unique labels.
c	Class counting function.
β_k	Class distribution of client k . $k = 0$ for overall class distribution.
ω_k	Delay time of client k relative to the fastest one.
$L(\mathcal{D}_0; \mathbf{w})$	Global loss function.
f	Model mapping function.
\mathbf{w}	Global model parameter vector.
$\mathbf{w}_s/\mathbf{w}_c$	Server/client model parameter vectors.
\mathcal{T}	Set of optimization steps. T in total.
$\mathcal{B}_k^{(t)}$	Local batch from client k at optimization step t .
B_k	Local batch size of client k .
$\mathcal{B}^{(t)}$	Global batch at optimization step t
B	Global batch size. $B = \sum_{k=1}^K B_k$.
$\mathbf{g}_{\mathbf{w}}^{(t)}$	Gradient vector of $L(\mathcal{B}^{(t)}; \mathbf{w})$.
E	Number of epochs/training rounds.

IV. PARALLEL SPLIT LEARNING WITH GLOBAL SAMPLING

A good sampling method should ensure that the expected distribution of the global batches aligns with the empirical distribution. If the global batches frequently deviate from the empirical distribution, the trained model may become biased and generalize poorly. We measure the quality of a sampling method by the deviation of the generated global batches from the empirical distribution, referred to as *batch-deviation*. By analyzing how the choice of local batch sizes affects the batch deviation, we determine the UGS method that is bounded at least as tight as to central uniform sampling in terms of batch deviation and decouples the effective batch size from the number of clients. All proofs are provided in Section B.

A. Deviation Analysis

Assume we are given the complete dataset \mathcal{D}_0 and train our model using central learning. In this scenario, the model is

typically trained using batches \mathcal{B} of size B that are sampled uniformly at random. Although uniform sampling does not guarantee minimal batch deviation, it is common due to its simplicity and efficiency. To simplify our analysis, we consider the overall class distribution β_0 instead of the empirical distribution, assuming that the class distribution acts as a proxy for the empirical distribution. We define the batch deviation as the L_1 distance between the class distribution of a batch \mathcal{B} with class label vector \mathbf{y} and β_0 :

$$d(\mathcal{B}, \beta_0) = \sum_{m=1}^M \left| \frac{c(\mathbf{y}, m)}{B} - \beta_{0,m} \right| \quad (1)$$

Let $Y = (Y_1, Y_2, \dots, Y_M)^\top$ be a random vector representing the class counts in a batch \mathcal{B} sampled from \mathcal{D}_0 uniformly at random with $Y \sim \text{Multinomial}(B, \beta_0)$. Using the Chebychev inequality, we can derive an upper bound on the probability of \mathcal{B} deviating from β_0 by at least ϵ :

Lemma 1. *For all $\epsilon > 0$ and $m \in \mathcal{M}$ it holds that*

$$P\left(\left|\frac{Y_m}{B} - \beta_{0,m}\right| \geq \epsilon\right) \leq \frac{\text{Var}(Y_m)}{B^2 \epsilon^2}$$

Our goal is to determine a sampling method for PSL with a deviation bound at least as tight as the one from central uniform sampling. In the regular PSL framework, a local batch size B_k is assigned to each client k and does not change during training. The class distribution of each local batch \mathcal{B}'_k is modelled as a multinomial distribution with parameters B_k and β_k . Let $Y' = (Y'_1, Y'_2, \dots, Y'_M)^\top$ be a random vector representing the class counts in the corresponding global batch \mathcal{B}' . Since the \mathcal{B}'_k are sampled independently, Y' is distributed according to the sum of the multinomials:

$$Y' \sim \sum_{k=1}^K \text{Multinomial}(B_k, \beta_k)$$

Using the Markov inequality, we can derive an upper bound on the probability of \mathcal{B}' deviating from β_0 by at least ϵ and relate it to \mathcal{B} , i.e., batches generated by central uniform sampling:

Lemma 2. *For all $\epsilon > 0$ and $m \in \mathcal{M}$ it holds that*

$$P\left(\left|\frac{Y'_m}{B} - \beta_{0,m}\right| \geq \epsilon\right) \leq \frac{\text{Var}(Y'_m) + (\mathbb{E}[Y'_m] - \mathbb{E}[Y_m])^2}{B^2 \epsilon^2}$$

The upper bound loosens when the bias term $(\mathbb{E}[Y'_m] - \mathbb{E}[Y_m])^2$ increases. Since $\mathbb{E}[Y'_m] = \sum_{k=1}^K B_k \beta_{k,m}$ and $\mathbb{E}[Y_m] = B \beta_{0,m}$, this implies that even small differences in the B_k or $\beta_{k,m}$ can lead to a significant deviation in the global batches.

Theorem 1. *If $B_k = B \frac{D_k}{D_0}$ or $\beta_{k,m} = \beta_{0,m}$ for all $k \in \mathcal{K}$ and $m \in \mathcal{M}$ then it holds that*

$$P\left(\left|\frac{Y'_m}{B} - \beta_{0,m}\right| \geq \epsilon\right) \leq \frac{\text{Var}(Y_m)}{B^2 \epsilon^2}$$

for all $m \in \mathcal{M}$.

Theorem 1 shows that choosing the B_k proportionally to the local dataset sizes ensures that the upper bound is at least as tight as the one from central uniform sampling in Lemma 1. Only if the client datasets are IID ($\beta_{k,m} = \beta_{0,m}$), any viable choice of local batch sizes B_k ensures the tightness of the deviation bound. Therefore, choosing the same local batch size $B_k = B'$ for all clients k as in [27] can lead to an increased batch deviation when the client datasets are non-IID. On the other hand, if $B \frac{D_k}{D_0} \notin \mathbb{N}$, the local batch sizes must be converted to integers. This can increase the deviation of the global batches in a non-IID setting, since the premise of Theorem 1 may not hold anymore throughout the training process.

B. Uniform Global Sampling (UGS)

We propose the UGS method, which ensures that Theorem 1 holds independent of local dataset sizes or local data distributions. The complete UGS method is outlined in Algorithm 1. In UGS, the local batch sizes are variable and determined by the server for each training step separately. It is not required to fix the local batch sizes right from the start. The server only requires a global batch size B to be specified.

UGS is invoked before each epoch of PSL. Each client k receives a local batch size vector $(B_k^{(1)}, B_k^{(2)}, \dots, B_k^{(T)})^\top$ from the server such that $\sum_{k=1}^K B_k^{(t)} = B$ for all $t \in \mathcal{T}$. The $B_k^{(t)}$ specify the local batch size of client k at training step t . If $B_k^{(t)} = 0$, the client k does not contribute to the global batch at training step t . UGS uses the following generative process to sample the global batches $\mathcal{B}^{(t)}$ in each training step t :

- 1) Choose $\pi = \left(\frac{D_1}{D}, \frac{D_2}{D}, \dots, \frac{D_K}{D}\right)^\top$
- 2) For each $i \in \{1, 2, \dots, B\}$:
 - a) Choose a client $z_i^{(t)} \sim \text{Categorical}(\pi)$
 - b) Choose a class $y_i^{(t)} \sim \text{Categorical}(\beta_{z_i^{(t)}})$

The key idea is to first sample a client $z_i^{(t)} \in \mathcal{K}$ according to a categorical distribution with parameters π and then sample a class $y_i^{(t)} \in \mathcal{M}$ from the chosen client. Since $\sum_{k=1}^K \pi_k = 1$, UGS corresponds to sampling from a mixture of categorical distributions with the mixing probabilities π . In our context, π can be interpreted as the *client selection probabilities*. Note that the categorical distribution is used iteratively instead of sampling in one step from the multinomial distribution. This is because the clients actually sample uniformly without replacement. If a client k has no data left, the server needs to update the client selection probabilities π by setting $\pi_k = 0$ and renormalizing the remaining probabilities before continuing the sampling process.

$\mathbf{z}^{(t)} = (z_1^{(t)}, z_2^{(t)}, \dots, z_B^{(t)})^\top$ are latent variables that represent the clients from which the $y_i^{(t)}$ are sampled. This allows the sampling process to be split between the server and the clients, where the server executes 2a) and the clients execute 2b). Since steps 2a) and 2b) are independent, we can postpone step 2b) and pre-compute the $B_k^{(t)}$ for all $k \in \mathcal{K}$ and $t \in \mathcal{T}$. Accordingly, we count the occurrences of each client k in $\mathbf{z}^{(t)}$ with $B_k^{(t)} = c(\mathbf{z}^{(t)}, k)$ right after step 2a). The server then sends the $B_k^{(t)}$ to the clients.

Once training starts, the clients can execute the step 2b) on demand, i.e., sampling local batches of size $B_k^{(t)}$. This equals substituting B_k with $B_k^{(t)}$ in the first step of PSL in Section III. The rest of the training process remains unchanged. Consequently, the effective batch size B becomes a hyperparameter that is no longer dependent on the number of clients or their respective dataset sizes, addressing the large effective batch size problem.

Corollary 1. Let $\boldsymbol{\pi} = \left(\frac{D_1}{D_0}, \frac{D_2}{D_0}, \dots, \frac{D_K}{D_0}\right)^\top$. If

$$Y'_m \sim B \sum_{k=1}^K \pi_k \text{Categorical}(\beta_k)$$

then

$$\mathbb{P}\left(\left|\frac{Y'_m}{B} - \beta_{0,m}\right| \geq \epsilon\right) \leq \frac{\text{Var}(Y_m)}{B^2 \epsilon^2}$$

for all $m \in \mathcal{M}$.

Corollary 1 shows that Theorem 1 holds for the global batches generated by this process. Therefor, UGS ensures that the batch deviation bound is as tight as the one from central uniform sampling even in the presence of non-IID data distributions.

Algorithm 1 Uniform Global Sampling

Input: $(D_1, \dots, D_K)^\top, B$

Output: $B_k^{(t)}$ for all $k \in \mathcal{K}$ and $t \in \mathcal{T}$

```

1:  $D \leftarrow \sum_{k=1}^K D_k$ 
2:  $T \leftarrow \lceil D/B \rceil$ 
3:  $B_k^{(t)} \leftarrow 0$  for all  $k \in \mathcal{K}$  and  $t \in \mathcal{T}$ 
4:
5:  $\boldsymbol{\pi} \leftarrow \left(\frac{D_1}{D}, \frac{D_2}{D}, \dots, \frac{D_K}{D}\right)^\top$ 
6:
7: for each training step  $t = 1$  to  $T$  do
8:   for  $i = 1$  to  $B$  do
9:      $z_i \sim \text{Categorical}(\boldsymbol{\pi})$ 
10:     $B_{z_i}^{(t)} \leftarrow B_{z_i}^{(t)} + 1$ 
11:    if  $\sum_{t'=1}^t B_{z_i}^{(t')} = D_{z_i}$  then
12:       $\pi_{z_i} \leftarrow 0$ 
13:       $\boldsymbol{\pi} \leftarrow \boldsymbol{\pi} / \sum_{k=1}^K \pi_k$ 
14:    end if
15:  end for
16: end for
17: return  $B_k^{(t)}$  for all  $k \in \mathcal{K}$  and  $t \in \mathcal{T}$ 

```

C. Straggler Mitigation

While UGS addresses the issue of large effective batch sizes and non-IID data distributions, it does not consider the presence of stragglers. Intuitively, by increasing the client selection probability π'_k of a straggler client k' , we can reduce the number of global batches to which the straggler client contributes. This reduces the total training time, as the straggler clients' datasets deplete faster and they appear less frequently in global batches.

However, adjusting the $\boldsymbol{\pi}$ can increase the batch deviation, as Corollary 1 would no longer hold. The choice of $\boldsymbol{\pi}$ is thus crucial to balance the trade-off between the batch deviation and the concentration of stragglers in the global batches. To address this issue, we treat $\boldsymbol{\pi}$ as a parameter to be optimized with respect to the desired trade-off. Inspired by the Latent Dirichlet Allocation model [28], we introduce a Dirichlet prior distribution over $\boldsymbol{\pi}$ with concentration parameter $\boldsymbol{\alpha} \in \mathbb{R}^K$ and $\alpha_k > 0$. As a conjugate to the categorical distribution, the Dirichlet distribution is a suitable choice for the prior distribution. The choice of $\boldsymbol{\alpha}$ is crucial to balance the trade-off between batch deviation and total training time. For now we assume that $\boldsymbol{\alpha}$ is given and will discuss its initialization in the next subsection. The prior distribution over $\boldsymbol{\pi}$ is defined as:

$$P(\boldsymbol{\pi} | \boldsymbol{\alpha}) = \frac{1}{B(\boldsymbol{\alpha})} \prod_{k=1}^K \pi_k^{\alpha_k - 1}$$

where $B(\boldsymbol{\alpha})$ is the Beta function. Furthermore we have:

$$p(z | \boldsymbol{\pi}) = \pi_z \quad \text{and} \quad p(y | z, \boldsymbol{\beta}) = \beta_{z,y}$$

The goal is to estimate the mixture proportions $\boldsymbol{\pi}^*$ that maximize the posterior distribution $P(\boldsymbol{\pi} | \mathbf{y}, \boldsymbol{\alpha}, \boldsymbol{\beta})$, so that the global batches that are generated using $\boldsymbol{\pi}^*$ are less likely to deviate from \mathbf{y} while respecting the prior beliefs given by $\boldsymbol{\alpha}$. Here $\mathbf{y} \in \mathcal{M}^N$ with sample size $N \in \mathbb{N}$ is the observed and incomplete data we want to fit our model to. For an accurate estimation the class distribution of \mathbf{y} should match the overall class distribution as closely as possible. This can be formulated as a MAP estimation problem:

$$\begin{aligned}
\boldsymbol{\pi}^* &= \arg \max_{\boldsymbol{\pi}} P(\boldsymbol{\pi} | \mathbf{y}, \boldsymbol{\alpha}, \boldsymbol{\beta}) \\
&= \arg \max_{\boldsymbol{\pi}} P(\mathbf{y} | \boldsymbol{\pi}, \boldsymbol{\beta}) \cdot P(\boldsymbol{\pi} | \boldsymbol{\alpha}) \\
&= \arg \max_{\boldsymbol{\pi}} \ln P(\mathbf{y} | \boldsymbol{\pi}, \boldsymbol{\beta}) + \ln P(\boldsymbol{\pi} | \boldsymbol{\alpha}) \\
&= \arg \max_{\boldsymbol{\pi}} \ln \left\{ \sum_{z \in \mathcal{K}^N} P(\mathbf{y}, z | \boldsymbol{\pi}, \boldsymbol{\beta}) \right\} + \ln P(\boldsymbol{\pi} | \boldsymbol{\alpha})
\end{aligned} \tag{2}$$

Due to the sum inside the logarithm in Equation (2), a closed-form solution for the MAP estimate is not available. Instead, we use the Expectation-Maximization (EM) algorithm [29] to iteratively estimate the mixture proportions $\boldsymbol{\pi}^*$.

The EM algorithm is a two-step iterative optimization algorithm that alternates between the Expectation (E) step and the Maximization (M) step to seek the maximum likelihood estimate of a marginal likelihood function. We use the MAP variant of the EM algorithm. It starts with an initial parameter value $\boldsymbol{\pi}^{\text{old}} \sim P(\boldsymbol{\pi} | \boldsymbol{\alpha})$ and iteratively refines the estimate until convergence. The E-step computes the expected value of the log likelihood $P(\mathbf{y}, z | \boldsymbol{\pi}, \boldsymbol{\beta})$ w.r.t. $\boldsymbol{\pi}^{\text{old}}$ and is given by:

$$\begin{aligned}
\mathcal{Q}(\boldsymbol{\pi}, \boldsymbol{\pi}^{\text{old}}) &= \mathbb{E}_{\mathbf{z}} \left[\ln P(\mathbf{y}, \mathbf{z} \mid \boldsymbol{\pi}, \boldsymbol{\beta}) \right] \\
&= \sum_{\mathbf{z} \in \mathcal{K}^N} P(\mathbf{z} \mid \mathbf{y}, \boldsymbol{\pi}^{\text{old}}, \boldsymbol{\beta}) \ln P(\mathbf{y}, \mathbf{z} \mid \boldsymbol{\pi}, \boldsymbol{\beta}) \\
&= \sum_{\mathbf{z} \in \mathcal{K}^N} P(\mathbf{z} \mid \mathbf{y}, \boldsymbol{\pi}^{\text{old}}, \boldsymbol{\beta}) \ln \{P(\mathbf{y} \mid \mathbf{z}, \boldsymbol{\beta})P(\mathbf{z} \mid \boldsymbol{\pi})\} \\
&= \sum_{n=1}^N \sum_{k=1}^K \gamma_{nk} \{ \ln \pi_k + \ln \beta_{k,y_n} \} \quad (3)
\end{aligned}$$

Note that we use the expected value of the posterior distribution $P(\mathbf{z} \mid \mathbf{y}, \boldsymbol{\pi}^{\text{old}}, \boldsymbol{\beta})$ in Equation (3) since the latent variables \mathbf{z} are not observed. The responsibilities γ_{nk} are given by:

$$\gamma_{nk} = \frac{\pi_k^{\text{old}} \beta_{k,y_n}}{\sum_{k' \in \mathcal{K}} \pi_{k'}^{\text{old}} \beta_{k',y_n}}$$

In the M-step, \mathcal{Q} is maximized with respect to $\boldsymbol{\pi}$. Adding the log prior $\ln P(\boldsymbol{\pi} \mid \boldsymbol{\alpha})$ to the objective function is the only modification required to use the EM algorithm for MAP estimation [29]. The M-step is given by:

$$\boldsymbol{\pi}^{\text{new}} = \arg \max_{\boldsymbol{\pi}} \mathcal{Q}(\boldsymbol{\pi}, \boldsymbol{\pi}^{\text{old}}) + \ln P(\boldsymbol{\pi}) \quad (4)$$

Solving the maximization problem yields the following update rule:

Proposition 1. *The M-step for Equation (4) has a closed-form solution and is given by:*

$$\pi_k^{\text{new}} = \frac{N_k + \alpha_k - 1}{N + \alpha_0 - K}$$

where $N_k = \sum_{n=1}^N \gamma_{nk}$ and $\alpha_0 = \sum_{k=1}^K \alpha_k$.

Afterwards, $\boldsymbol{\pi}^{\text{old}}$ is updated to $\boldsymbol{\pi}^{\text{new}}$ and the E- and M-steps are iteratively repeated until convergence. The convergence is achieved once $\|\boldsymbol{\pi}^{\text{new}} - \boldsymbol{\pi}^{\text{old}}\|_2 < \tau$, where $\tau > 0$ is the convergence threshold hyperparameter. Once the algorithm converges, the MAP estimate $\boldsymbol{\pi}^* = \boldsymbol{\pi}^{\text{new}}$ is obtained. $\boldsymbol{\pi}^*$ is guaranteed to be a local maximum of the posterior distribution $P(\boldsymbol{\pi} \mid \mathbf{y}, \boldsymbol{\alpha}, \boldsymbol{\beta})$. The complete EM algorithm for the MAP estimation is outlined in Algorithm 2.

Note that since $y_n = y_{n'} \implies \gamma_{nk} = \gamma_{n'k}$ for $n, n' \in \{1, 2, \dots, N\}$, the responsibilities γ_{nk} can be precomputed for each class $m \in \mathcal{M}$. We define $\Gamma_k \in \mathbb{R}^M$ as the classwise responsibilities for client k with

$$\Gamma_{k,m} = \frac{\pi_k^{\text{old}} \beta_{k,m}}{\sum_{k' \in \mathcal{K}} \pi_{k'}^{\text{old}} \beta_{k',m}} \quad (5)$$

and $\boldsymbol{\nu} \in \mathbb{N}^M$ as the class counts in \mathbf{y} with $\nu_m = (c(\mathbf{y}, 1), c(\mathbf{y}, 2), \dots, c(\mathbf{y}, M))^{\top}$.

This allows us to reformulate the term N_k in the M-step as $N_k = \boldsymbol{\nu}^{\top} \Gamma_k$. The class counts $\boldsymbol{\nu}$ need to be computed only once at the beginning of the EM algorithm and Γ_k involves the computation of $M \cdot K$ responsibilities per iteration. In the original formulation, $N \cdot K$ responsibilities need to be computed per iteration. Since usually $M \ll N$, this

reformulation can lead to a significant speedup. This means that we can take advantage of the complete dataset \mathcal{D}_0 by choosing $\mathbf{y} = \mathbf{y}_0$ for a more accurate estimation of $\boldsymbol{\pi}^*$ without additional computational cost compared to using an N -sized sample (except for the computation of $\boldsymbol{\nu}$, which is negligible).

Algorithm 2 EM Algorithm for MAP Estimation

Input: $\mathbf{y}, \boldsymbol{\pi}, \boldsymbol{\beta}, \boldsymbol{\alpha}, \tau$

Output: $\boldsymbol{\pi}^*$

- 1: $\boldsymbol{\pi}^{\text{old}} \leftarrow \boldsymbol{\pi} \cdot \infty$
 - 2: $\boldsymbol{\pi}^{\text{new}} \leftarrow \boldsymbol{\pi}$
 - 3: $N \leftarrow |\mathbf{y}|$
 - 4: $\alpha_0 \leftarrow \sum_{k=1}^K \alpha_k$
 - 5: $\boldsymbol{\nu} \leftarrow (c(\mathbf{y}, 1), c(\mathbf{y}, 2), \dots, c(\mathbf{y}, M))^{\top}$
 - 6:
 - 7: **while** $\|\boldsymbol{\pi}^{\text{new}} - \boldsymbol{\pi}^{\text{old}}\|_2 \geq \tau$ **do**
 - 8: $\boldsymbol{\pi}^{\text{old}} \leftarrow \boldsymbol{\pi}^{\text{new}}$
 - 9: **for** $k = 1$ to K **do**
 - 10: Compute Γ_k using (5)
 - 11: $N_k \leftarrow \boldsymbol{\nu}^{\top} \Gamma_k$ ▷ E-Step
 - 12: $\pi_k^{\text{new}} \leftarrow \frac{N_k + \alpha_k - 1}{N + \alpha_0 - K}$ ▷ M-Step
 - 13: **end for**
 - 14: **end while**
 - 15: **return** $\boldsymbol{\pi}^{\text{new}}$
-

D. Initialization of Concentration Parameters

The EM algorithm is sensitive to the initialization of the parameters and may converge to different local maxima depending on the initialization. We initialize $\boldsymbol{\alpha}$ in two steps. First, we set $\alpha_k = \frac{D_k}{D} \cdot N$. This initial step is independent of the stragglers and provides a good starting point for optimization. The expected value for π_k with this initialization is $\frac{D_k}{D}$, which aligns with Corollary 1 and ensures that the π_k are most likely proportional to the dataset sizes. Our heuristic initialization keeps the α_k values in a range where they neither dominate the N_k in Proposition 1 nor are they insignificant, ensuring $N_k \leq \alpha_k$.

In the second step, we adjust the α_k for each client k to account for the delay times given a hyperparameter $\Delta \geq 0$:

$$\alpha_k \leftarrow \alpha_k \cdot \exp\left\{\Delta \cdot \frac{(\omega_k - \bar{\omega})}{s_{\omega}}\right\}$$

where $\bar{\omega} = \frac{1}{K} \sum_{k=1}^K \omega_k$ and $s_{\omega} = \sqrt{\frac{1}{K-1} \sum_{k=1}^K (\omega_k - \bar{\omega})^2}$

In this adjustment, the z-score $\frac{\omega_k - \bar{\omega}}{s_{\omega}}$ standardizes the delay times ω_k by measuring how many standard deviations each delay time is from the mean delay time $\bar{\omega}$. By incorporating the z-score into the exponential function, we achieve a smooth adjustment that either increases or decreases α_k based on the relative delay time of each client. Δ is the single hyperparameter that controls the trade-off between the batch deviation and the total training time. It changes the unit of measurement of the z-score in terms of standard deviations. Higher values of Δ lead to a more aggressive adjustment of the α_k and can

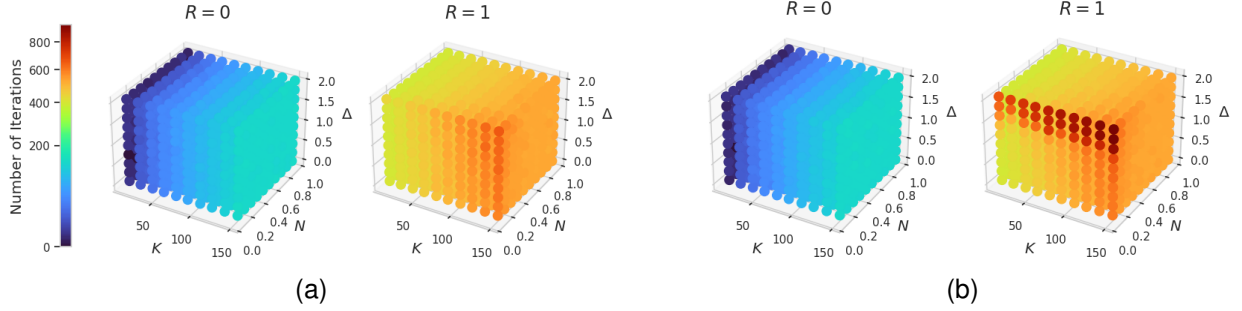


Fig. 2. Number of EM iterations in LDS for different parameter choices. N is given relative to D_0 . (a) $p_s = 0.1$ (b) $p_s = 0.2$

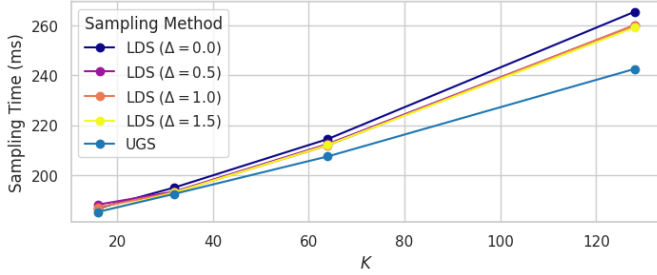


Fig. 3. Sampling time for UGS and LDS with different Δ .

reduce the total training time, but may also increase the batch deviation and vice versa.

E. Latent Dirichlet Sampling (LDS)

We introduce the LDS method that balances the trade-off between batch deviation and total training time. LDS is detailed in Algorithm 3. The procedure is almost identical to UGS, but differs in a few aspects.

First, the client selection probabilities π are estimated using the EM algorithm for MAP estimation as described in the previous section. Therefore the trade-off hyperparameter Δ needs to be provided. The concentration parameter α is initialized as described in the previous section. Note that for $\Delta = 0$, the delay times have no impact on α_k and the initialization is equivalent to the first step. In this case, the EM algorithm will almost surely converge to the same π as in UGS. Therefore, UGS can be seen as a special case of LDS with $\Delta = 0$.

Second, the π can not be simply renormalized after the dataset of a client k depletes. Instead, the component k is removed from the model and the remaining π are re-estimated to ensure that π remains a maximum of the posterior distribution. The choice for π at the beginning of the re-estimation is a crucial factor for the convergence speed of the EM algorithm. We differentiate between two cases based on the hyperparameter $R \in \{0, 1\}$. For $R = 1$, we sample π from the prior distribution $P(\pi | \alpha)$ as starting point (re-initialization). For $R = 0$, we use the last π as starting point (no re-initialization). The choice of R has a significant impact on the convergence speed of the EM algorithm. We provide empirical results in the next section.

Algorithm 3 Latent Dirichlet Sampling

Input: $(D_1, \dots, D_K)^\top, \beta, \omega, B, \mathbf{y}$

Input: Δ, τ, R

▷ Hyperparameters

Output: $B_k^{(t)}$ for all $k \in \mathcal{K}$ and $t \in \mathcal{T}$

1: $D \leftarrow \sum_{k=1}^K D_k$

2: $T \leftarrow \lceil D/B \rceil$

3: $B_k^{(t)} \leftarrow 0$ for all $k \in \mathcal{K}$ and $t \in \mathcal{T}$

4:

5: $\alpha \leftarrow (\frac{D_1}{D}, \frac{D_2}{D}, \dots, \frac{D_K}{D})^\top$

6: **for** $k = 1$ to K **do**

7: $\alpha_k \leftarrow \alpha_k \cdot \exp\{\Delta \cdot \frac{(\omega_k - \bar{\omega})}{s_\omega}\}$

8: **end for**

9: $\pi \sim \text{Dir}(\alpha)$

10: $\pi \leftarrow \text{EmMap}(\mathbf{y}, \pi, \beta, \alpha, \tau)$

11:

12: **for** each training step $t = 1$ to T **do**

13: **for** $i = 1$ to B **do**

14: $z_i \sim \text{Categorical}(\pi)$

15: $B_{z_i}^{(t)} \leftarrow B_{z_i}^{(t)} + 1$

16: **if** $\sum_{t'=1}^t B_{z_i}^{(t')} = D_{z_i}$ **then**

17: $\beta, \pi, \alpha \leftarrow \text{RemoveComponent}(z_i, \beta, \pi, \alpha)$

18:

19: **if** $R = 1$ **then**

20: $\pi \sim \text{Dir}(\alpha)$

21: **end if**

22:

23: $\pi \leftarrow \text{EmMap}(\mathbf{y}, \pi, \beta, \alpha, \tau)$

24: **end if**

25: **end for**

26: **end for**

27: **return** $B_k^{(t)}$ for all $k \in \mathcal{K}$ and $t \in \mathcal{T}$

V. SIMULATION RESULTS

This section provides a comprehensive evaluation of the proposed UGS and LDS methods in terms of model performance and training time. We compare PSL extended by our sampling methods with several existing frameworks, focusing on metrics such as test accuracy, convergence behavior, and Time-Per-Epoch (TPE). Furthermore, we investigate the effectiveness of LDS for mitigating stragglers, and analyze its time complexity under various conditions.

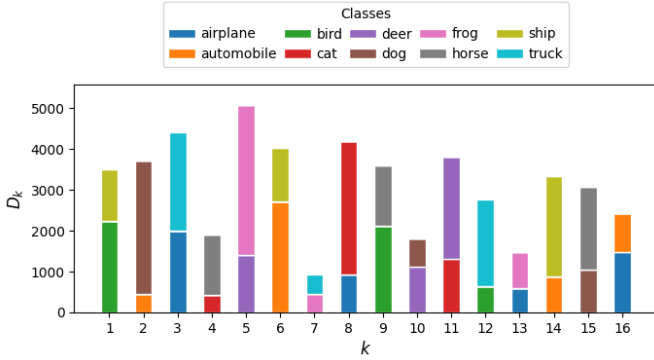


Fig. 4. Example of a Non-IID setting for $K = 16$ clients.

A. Model Performance and Training Time

We trained a ResNet18 [38] model on the CIFAR10 [39] dataset using PSL with the proposed UGS and LDS (with $\Delta = 0.0$) in the absence of stragglers. We compared the test accuracy with PSL using fixed and proportional local batch sizes like in [22]. For brevity we refer to this default sampling method as Fixed Proportional Local Sampling (FPLS). If the local batch sizes are fixed and identical like in [27], we refer to this sampling method as Fixed Local Sampling (FLS). To ensure that all local batch sizes are integer, we round them to the nearest integer. If the nearest integer is 0, we set the batch size to 1 to ensure that each client contributes to the training process. We also include other frameworks, namely SL, FL, and SFL, as well as central learning (CL) as a baseline. The hyperparameter choices, hardware setup, and training details can be found in Section A.

We split the datasets either in an IID or non-IID manner, while considering different numbers of clients $K \in \{16, 32, 64, 128\}$. To achieve a non-IID split, a Dirichlet-based data partition method is used, similar to the Extended Dirichlet Strategy in [16]. The method is applied to the datasets such that each client has exactly 2 classes with strongly varying dataset sizes, simulating strong heterogeneity among the clients. The resulting client datasets are shown exemplary in Figure 4 for $K = 16$ clients. We trained the model for 100 epochs with a global batch size of $B = 128$ and report the maximum test accuracy achieved during training in Table II. Accuracies are averaged over 5 runs with different random seeds and given in percentages. The best accuracy for each split and K is highlighted in boldface. The non-IID split is denoted as (IID) in the table. CL achieved a maximum accuracy of 90.25%. In Figure 5, we show the test accuracy per epoch for a run with $K = 128$.

We observe that PSL with UGS and LDS significantly outperforms the other frameworks in terms of test accuracy. Compared to PSL with FPLS, UGS and LDS increase the test accuracy by up to 34.1% in the non-IID setting. Our proposed methods achieved a test accuracy close to the central learning baseline in both IID and non-IID settings, in some cases even surpassing it. The other frameworks show a significant drop in test accuracy in the non-IID setting and strong fluctuations, suggesting that the model training is unstable. The fluctuations

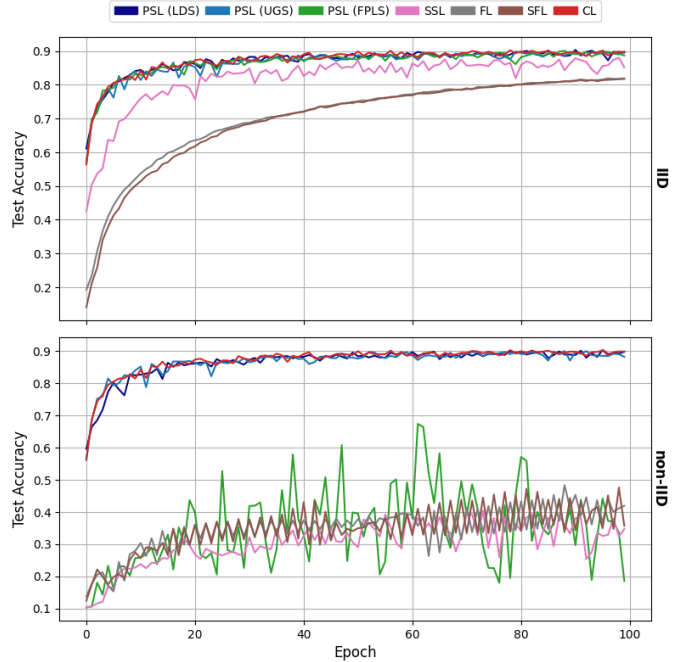


Fig. 5. Test accuracy per epoch for different frameworks training ResNet18 on CIFAR10 in IID and Non-IID settings.

are particularly pronounced for PSL with FPLS. In contrast, PSL with UGS and LDS shows a stable convergence behavior. The accuracies achieved by UGS and LDS are closely aligned. The results suggest that UGS and LDS are effective in mitigating the challenges of large effective batch sizes and non-IID data in PSL.

To investigate the performance gap between our methods and PSL with fixed local batch sizes, we compared the batch deviation (as defined in Equation (1)) of UGS with FPLS and FLS. We calculated the mean and standard deviation of the batch deviation in the global batch sequence generated by the different methods. We considered different values of B and K under IID and non-IID settings, as shown in Figure 6. In the IID scenario, all sampling strategies exhibited nearly identical means and standard deviations. This is consistent with Theorem 1, since $\beta_{0,m} \approx \beta_{k,m}$ for all k and m . Differences between UGS, FPLS, and FLS were minimal, with UGS maintaining a nearly constant mean and standard deviation in both IID and non-IID cases. However, FPLS and FLS showed a marked increase in mean and standard deviation in the non-IID scenario. The worst batch deviation in non-IID cases was observed with FLS, while FPLS showed a lower mean and standard deviation that decreased with higher K , though still considerably higher than UGS. For UGS, a larger batch size consistently reduced both mean and standard deviation in both IID and non-IID cases, aligning with the deviation bound in Lemma 1. In contrast, for FPLS and FLS, this reduction was observed only in the IID case. This suggests the dominance of the bias term in the deviation bound of Lemma 2 in the non-IID setting. Our findings suggests that sampling methods with fixed local batch sizes introduce greater batch deviation to the training process, explaining the performance gap between

TABLE II
TEST ACCURACIES FOR DIFFERENT FRAMEWORKS

Test Acc.	PSL (UGS)		PSL (LDS)		PSL (FPLS)		FL		SFL		SSL	
	IID	$\overline{\text{IID}}$	IID	$\overline{\text{IID}}$	IID	$\overline{\text{IID}}$	IID	$\overline{\text{IID}}$	IID	$\overline{\text{IID}}$	IID	$\overline{\text{IID}}$
$K \downarrow$												
16	90.43	90.24	89.85	90.80	89.89	87.14	87.65	44.20	88.10	48.04	90.18	21.26
32	90.75	89.98	90.66	89.90	90.05	74.52	86.31	49.84	86.96	49.71	90.68	33.18
64	90.11	90.17	90.21	90.72	90.26	71.75	84.33	48.65	84.77	53.87	90.53	30.92
128	90.10	89.95	90.37	90.28	90.07	67.32	81.96	48.34	81.80	47.59	88.06	40.40

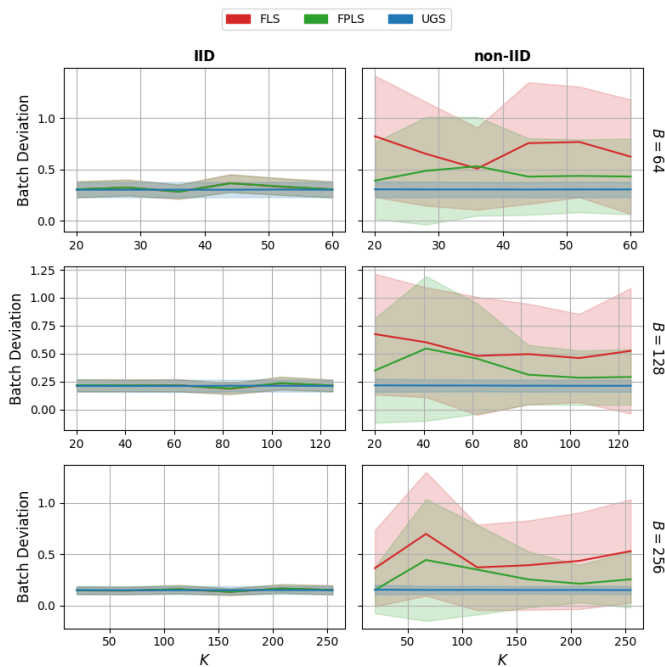


Fig. 6. Mean and standard deviation of the batch deviation for UGS, FLS, and FPLS using different K and B .

UGS and FPLS.

B. Evaluation of LDS for Straggler Mitigation

To evaluate the effectiveness of the LDS method for straggler mitigation, we introduced stragglers into the training process by defining a straggler probability p_s , a minimum straggler delay ω_{\min} , and a maximum straggler delay ω_{\max} . We randomly selected a subset of clients to be stragglers with probability p_s and introduced a delay ω uniformly distributed between ω_{\min} and ω_{\max} . For non-stragglers the delay time was set to zero. Each client k waited for ω_k milliseconds before sending its data to the server. We trained the model again on the CIFAR10 dataset with the same hyperparameters using PSL with LDS. We measured the TPE for different straggler probabilities $p_s \in \{0.1, 0.2, 0.3\}$ and $\Delta \in \{0.5, 1.0, 1.5\}$ under IID and non-IID dataset splits. The results are shown in ???. TPEs are averaged over the 5 runs and given in seconds. We included the TPE for $\Delta = 0.0$ in the absence of stragglers as a baseline. The best TPE for each split, K , and p_s is highlighted in boldface.

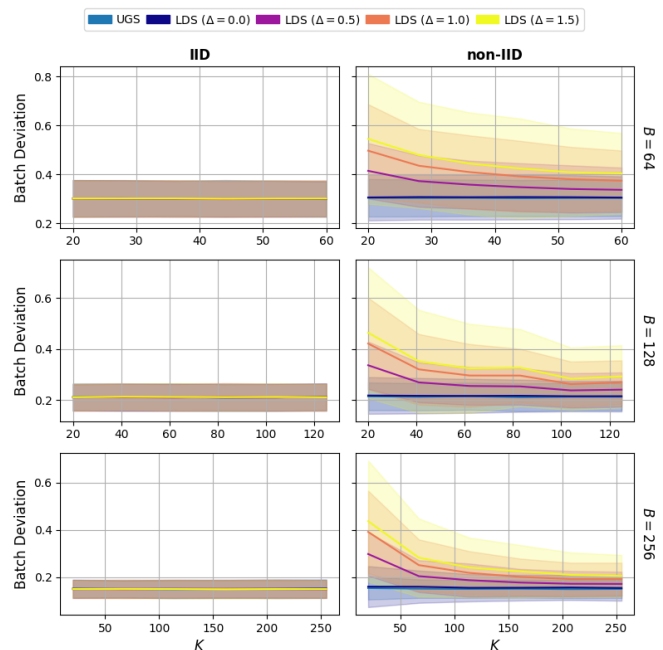


Fig. 7. Mean and standard deviation of the batch deviation for UGS and LDS using different Δ , K , and B .

For $p_s = 0.1$, the TPE increased drastically, especially for fewer clients K . Increasing p_s further only slightly increased the TPE. Higher Δ values significantly reduced the TPE by up to 62%. For $p_s = 0.1$ and $\Delta = 1.5$ the TPE was only slightly higher than without stragglers. Higher p_s made LDS less effective in reducing the TPE due to the increased straggler concentration in the global batch sequence, especially with fewer clients K . Figure 8 shows the processing times per batch and the total processing time for different p_s and Δ with $K = 128$ clients. Higher Δ led to faster decreases in the processing time. Higher p_s reduced the rate of this decrease, setting a lower bound beyond which Δ had no effect.

We compared test accuracy for each setting, as shown in Table III. Accuracies are averaged over 5 runs and given in percentages. The best accuracy for each split, K and p_s is highlighted in boldface. The test accuracy remained close to the UGS baseline across all p_s and Δ , demonstrating robustness.

We compared the batch deviation of UGS and LDS in the same settings as before, using different values for Δ , K , and B under IID and non-IID settings. The results are shown in Figure 7. The difference in batch deviation was

TABLE III
TEST ACCURACIES FOR PSL WITH LDS

Test Acc.	$p_s = 0.1$						$p_s = 0.2$						$p_s = 0.3$					
	$\Delta = 0.5$		$\Delta = 1.0$		$\Delta = 1.5$		$\Delta = 0.5$		$\Delta = 1.0$		$\Delta = 1.5$		$\Delta = 0.5$		$\Delta = 1.0$		$\Delta = 1.5$	
	IID	$\bar{\text{IID}}$																
$K \downarrow$																		
16	90.27	90.22	90.28	90.89	90.05	90.78	90.34	90.45	90.45	90.85	90.32	90.74	90.23	89.58	90.24	89.19	90.60	87.06
32	90.55	90.16	90.22	91.02	89.90	90.46	90.35	90.48	90.38	90.73	90.41	90.57	90.11	90.37	90.19	90.65	90.06	90.50
64	90.18	90.21	90.28	90.47	90.30	90.55	90.33	90.43	90.68	90.81	90.39	90.74	90.11	90.36	90.44	90.46	89.98	90.41
128	90.24	90.35	90.17	90.57	90.26	90.99	90.22	90.50	90.54	90.35	90.15	90.43	89.99	90.46	90.62	90.50	90.10	90.89

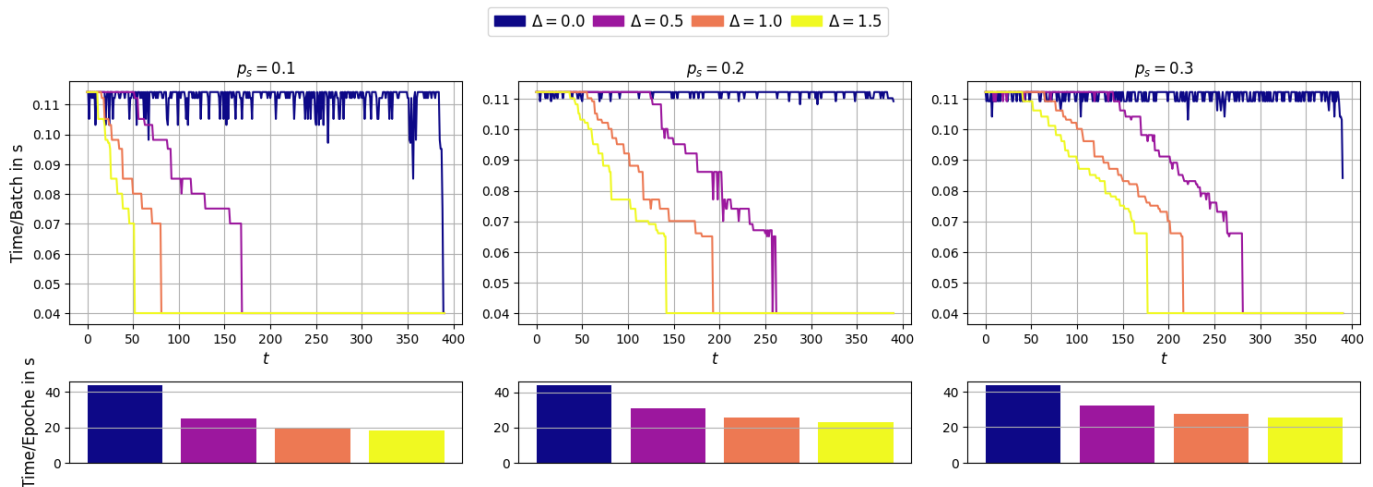


Fig. 8. Per-batch processing time and total time (i.e., TPE) in seconds for different p_s and Δ with $K = 128$ clients.

more pronounced than the difference in accuracy. In the IID case, the batch deviation was nearly identical for all cases. In the non-IID case, LDS with $\Delta = 0.0$ closely aligned with UGS. Higher Δ increased mean and standard deviation, but significantly less than FLS and FPLS. Mean and standard deviation decreased with higher K and B . The negligible effect on the model accuracy likely results from the low increase in batch deviation, which is not sufficient to impact the model training.

The significant TPE reduction without impacting accuracy, especially under a strong non-IID distribution, suggests that LDS is effective for straggler mitigation.

C. Time Complexity of LDS

We measured the total number of EM iterations invoked during LDS for various values of Δ , K , N , and R . We present our results for $p_s = 0.1$ and $p_s = 0.2$, respectively, as a 3D heatmap in Figure 2. We observe that reinitialization ($R = 1$) significantly impacts the number of iterations. Without reinitialization ($R = 0$), the EM algorithm requires on average less than a third of the iterations to converge. This indicates that the π from the previous iteration provides a good starting point for the next iteration. The highest number of iterations occurs when using $R = 1$ with a high value of Δ . The EM algorithm needs more iterations to converge when the α are adjusted more aggressively. Poor initial values due to reinitialization strongly exacerbates this effect. For a higher

number of clients K , the number of iterations increased in all cases. This is primarily because the EM algorithm must be re-run each time a client dataset depletes. The results show that the choice of sample size N has no significant impact on the number of iterations. This is due to the speedup achieved by the reformulation of the E-step in Section IV-C.

Lastly, we measure the total sampling time required for LDS and compare it with UGS. We use a straggler probability of $p_s = 0.2$, a batch size of $B = 128$, and different values of Δ . The results, shown in Figure 3, indicate that the sampling time for LDS increases as K increases. This is because the number of EM invocations and the number of computations for the Γ_k scales with K . However, LDS is still only slightly slower than UGS, even for high values of Δ . Thus, LDS not only provides a significant reduction in TPE but also maintains a low computational overhead compared to UGS.

D. Limitations

Our methods have several limitations. First, we assume that the delay times do not change significantly during an epoch. However, this assumption may not hold in practice. The straggler mitigation may not be effective if the delay times change frequently. Furthermore, the inherent reliance on gradient averaging causes increased latency and communication overhead. Gradient averaging exacerbates the straggler effect, as the server must wait for all contributing clients to send their gradients before proceeding. Lastly, we observed that when

the number of clients is at least as large as the global batch size, the local batch sizes can become very small, which leads to increased latency due to idle clients. The integration of UGS and LDS with other advanced techniques like local loss function design and client clustering could further enhance the performance of PSL, by removing the need for gradient averaging and improving the scalability of the framework.

VI. CONCLUSION

In this paper, we proposed the UGS and LDS methods as an extension to the PSL framework introduced in [22]. Our methods addressed key challenges in PSL, including large effective batch sizes, Non-IID data distributions, and the straggler effect. UGS mitigates the large effective batch size problem by allowing variable local batch sizes, decoupling the number of clients from the effective batch size. Our analysis demonstrated that UGS effectively reduces batch deviations, even under Non-IID data settings. LDS is a generalization of UGS and balances the trade-off between batch deviation and training time using a single hyperparameter Δ that controls the trade-off. Our extensive simulations on the CIFAR10 dataset showed that PSL with UGS and LDS outperforms existing frameworks in terms of test accuracy and convergence stability. Specifically, our methods achieved a test accuracy close to the central learning baseline in the Non-IID setting, while other frameworks experienced significant drops in performance. Compared to PSL with fixed local batch sizes, UGS and LDS increased the test accuracy by up to 34.1% in the Non-IID setting. The evaluation of LDS for straggler mitigation revealed substantial reduction in Time-Per-Epoch, achieving a reduction of up to 62%. Our findings suggest that UGS and LDS are promising solutions for enhancing PSL performance in real-world applications. Venues for future research include improving the client scalability, reducing the communication overhead, and decreasing the training latency of PSL.

REFERENCES

- [1] M. Z. Alom, T. M. Taha, C. Yakopcic, S. Westberg, P. Sidike, M. S. Nasrin, M. Hasan, B. C. Van Essen, A. A. S. Awwal, and V. K. Asari, "A State-of-the-Art Survey on Deep Learning Theory and Architectures," *Electronics*, vol. 8, no. 3, p. 292, Mar. 2019.
- [2] M. Kohankhaki, A. Ayad, M. Barhoush, B. Leibe, and A. Schmeink, "Radiopaths: Deep Multimodal Analysis on Chest Radiographs," *IEEE Int. Conf. Big Data*, pp. 3613–3621, Dec. 2022.
- [3] A. Ayad, M. Frei, and A. Schmeink, "Efficient and Private ECG Classification on the Edge Using a Modified Split Learning Mechanism," *2022 IEEE 10th Int. Conf. Healthcare Inform.*, pp. 01–06.
- [4] D. W. Otter, J. R. Medina, and J. K. Kalita, "A Survey of the Usages of Deep Learning for Natural Language Processing," *IEEE Trans. Neural Netw. Learn. Syst.*, vol. 32, no. 2, pp. 604–624, Feb. 2021.
- [5] M. Barhoush, A. Hallawa, A. Peine, L. Martin, and A. Schmeink, "Localization-Driven Speech Enhancement in Noisy Multi-Speaker Hospital Environments Using Deep Learning and Meta Learning," *IEEE/ACM Trans. Audio Speech Lang. Process.*, vol. 31, pp. 670–683, 2023.
- [6] J. Park, S. Samarakoon, M. Bennis, and M. Debbah, "Wireless Network Intelligence at the Edge," *Proc. IEEE*, vol. 107, no. 11, pp. 2204–2239, Nov. 2019.
- [7] Z. Zhou, X. Chen, E. Li, L. Zeng, K. Luo, and J. Zhang, "Edge Intelligence: Paving the Last Mile of Artificial Intelligence With Edge Computing," *Proc. IEEE*, vol. 107, no. 8, pp. 1738–1762, Aug. 2019.
- [8] J. Park, S. Wang, A. Elgabri, S. Oh, E. Jeong, H. Cha, H. Kim, S.-L. Kim, and M. Bennis, "Distilling On-Device Intelligence at the Network Edge," arXiv:1908.05895, Aug. 2019.
- [9] H. B. McMahan, E. Moore, D. Ramage, S. Hampson, and B. A. Y. Arcas, "Communication-Efficient Learning of Deep Networks from Decentralized Data," in *Int. Conf. Artif. Intell. and Statist.*, Feb. 2016.
- [10] K. Lee, M. Lam, R. Pedarsani, D. Papailiopoulos, and K. Ramchandran, "Speeding Up Distributed Machine Learning Using Codes," *IEEE Trans. Inform. Theory*, vol. 64, no. 3, pp. 1514–1529, Mar. 2018.
- [11] T. Nishio and R. Yonetani, "Client Selection for Federated Learning with Heterogeneous Resources in Mobile Edge," in *Proc. IEEE Int. Conf. Commun.*, May 2019, pp. 1–7.
- [12] F. Haddadpour, M. M. Kamani, A. Mokhtari, and M. Mahdavi, "Federated Learning with Compression: Unified Analysis and Sharp Guarantees," in *Int. Conf. Artif. Intell. and Statist.*, Jul. 2020.
- [13] P. Vepakomma, O. Gupta, T. Swedish, and R. Raskar, "Split learning for health: Distributed deep learning without sharing raw patient data," arXiv:1812.00564 [cs.LG], Dec. 2018.
- [14] M. Poirot, P. Vepakomma, K. Chang, J. Kalpathy-Cramer, R. Gupta, and R. Raskar, "Split Learning for collaborative deep learning in healthcare," arXiv:1912.12115 [cs.LG], Dec. 2019.
- [15] C. Thapa, M. A. P. Chamikara, and S. A. Camtepe, "Advancements of Federated Learning Towards Privacy Preservation: From Federated Learning to Split Learning," *Federated Learn. Syst.*, vol. 965, pp. 79–109, 2021.
- [16] Y. Li and X. Lyu, "Convergence analysis of sequential federated learning on heterogeneous data," in *Advances in Neural Inf. Process. Syst.*, vol. 36, 2023, pp. 56 700–56 755.
- [17] Y. Gao, M. Kim, S. Abuadba, Y. Kim, C. Thapa, K. Kim, S. A. Camtepe, H. Kim, and S. Nepal, "End-to-End Evaluation of Federated Learning and Split Learning for Internet of Things," *2020 Int. Symp. on Reliable Distrib. Syst.*, pp. 91–100.
- [18] J. Kirkpatrick, R. Pascanu, N. Rabinowitz, J. Veness, G. Desjardins, A. A. Rusu, K. Milan, J. Quan, T. Ramalho, A. Grabska-Barwinska, D. Hassabis, C. Clopath, D. Kumaran, and R. Hadsell, "Overcoming catastrophic forgetting in neural networks," *Proc. Natl. Acad. Sci. U.S.A.*, vol. 114, no. 13, pp. 3521–3526, Mar. 2017.
- [19] C. Thapa, P. C. Mahawaga Arachchige, S. Camtepe, and L. Sun, "SplitFed: When Federated Learning Meets Split Learning," *AAAI*, vol. 36, no. 8, pp. 8485–8493, Jun. 2022.
- [20] M. Gawali, C. S. Arvind, S. Suryavanshi, H. Madaan, A. Gaikwad, K. N. Bhanu Prakash, V. Kulkarni, and A. Pant, "Comparison of Privacy-Preserving Distributed Deep Learning Methods in Healthcare," *Med. Image Understanding and Analysis*, vol. 12722, pp. 457–471, 2021.
- [21] Y. Gao, M. Kim, C. Thapa, A. Abuadba, Z. Zhang, S. Camtepe, H. Kim, and S. Nepal, "Evaluation and Optimization of Distributed Machine Learning Techniques for Internet of Things," *IEEE Trans. Comput.*, vol. 71, no. 10, pp. 2538–2552, Oct. 2022.
- [22] J. Jeon and J. Kim, "Privacy-Sensitive Parallel Split Learning," in *2020 International Conference on Information Networking (ICOIN)*, pp. 7–9.
- [23] W. Wu, M. Li, K. Qu, C. Zhou, X. Shen, W. Zhuang, X. Li, and W. Shi, "Split Learning Over Wireless Networks: Parallel Design and Resource Management," *IEEE J. Select. Areas Commun.*, vol. 41, no. 4, pp. 1051–1066, Apr. 2023.
- [24] Z. Lin, G. Zhu, Y. Deng, X. Chen, Y. Gao, K. Huang, and Y. Fang, "Efficient Parallel Split Learning over Resource-constrained Wireless Edge Networks," arXiv:2303.15991 [cs.LG], 2023.
- [25] S. Oh, J. Park, P. Vepakomma, S. Baek, R. Raskar, M. Bennis, and S.-L. Kim, "LocFedMix-SL: Localize, Federate, and Mix for Improved Scalability, Convergence, and Latency in Split Learning," *Proc. of the ACM Web Conf.*, pp. 3347–3357, Apr. 2022.
- [26] D.-J. Han, H. I. Bhatti, J. Lee, and J. Moon, "Accelerating Federated Learning with Split Learning on Locally Generated Losses," in *ICML Workshop on Federated Learn. for User Privacy and Data Confidentiality*, 2021.
- [27] S. Pal, M. Uniyal, J. Park, P. Vepakomma, R. Raskar, M. Bennis, M. Jeon, and J. Choi, "Server-Side Local Gradient Averaging and Learning Rate Acceleration for Scalable Split Learning," arXiv:2112.05929 [cs.LG], Dec. 2021.
- [28] D. Blei, A. Ng, and M. Jordan, "Latent Dirichlet Allocation," in *Advances in Neural Inf. Process. Syst.*, vol. 14. MIT Press, 2001.
- [29] A. P. Dempster, N. M. Laird, and D. B. Rubin, "Maximum Likelihood from Incomplete Data Via the EM Algorithm," *J. of the Roy. Statist. Soc.*, vol. 39, no. 1, pp. 1–22, Sep. 1977.
- [30] "Mohkoh19/GPSL," <https://github.com/mohkoh19/GPSL>.
- [31] X. Lyu, S. Liu, J. Liu, and C. Ren, "Scalable Aggregated Split Learning for Data-Driven Edge Intelligence on Internet-of-Things," *IEEE Internet Things M.*, vol. 6, no. 4, pp. 124–129, Dec. 2023.

- [32] N. Golmant, N. Vemuri, Z. Yao, V. Feinberg, A. Gholami, K. Rothauge, M. W. Mahoney, and J. E. Gonzalez, "On the Computational Inefficiency of Large Batch Sizes for Stochastic Gradient Descent," arXiv:1811.12941 [cs.LG], Sep. 2018.
- [33] D. Wilson and T. R. Martinez, "The general inefficiency of batch training for gradient descent learning," *Neural Networks*, vol. 16, no. 10, pp. 1429–1451, Dec. 2003.
- [34] Y. Cai and T. Wei, "Efficient Split Learning with Non-iid Data," in *2022 23rd IEEE Int. Conf. on Mobile Data Manage.*, pp. 128–136.
- [35] M. Kim, A. DeRieux, and W. Saad, "A Bargaining Game for Personalized, Energy Efficient Split Learning over Wireless Networks," in *2023 IEEE Wireless Commun. and Netw. Conf.* Glasgow, United Kingdom: IEEE, pp. 1–6.
- [36] M. Zhang, J. Cao, Y. Sahni, X. Chen, and S. Jiang, "Resource-efficient Parallel Split Learning in Heterogeneous Edge Computing," in *2024 Int. Conf. on Comput., Netw. and Commun.* Big Island, HI, USA: IEEE, pp. 794–798.
- [37] E. Yang, D.-K. Kang, and C.-H. Youn, "BOA: Batch orchestration algorithm for straggler mitigation of distributed DL training in heterogeneous GPU cluster," *J Supercomput*, vol. 76, no. 1, pp. 47–67, Jan. 2020.
- [38] K. He, X. Zhang, S. Ren, and J. Sun, "Deep Residual Learning for Image Recognition," *2016 IEEE Conf. on Comput. Vis. and Pattern Recognit.*, pp. 770–778.
- [39] A. Krizhevsky, "Learning Multiple Layers of Features from Tiny Images," University of Toronto, Technical Report, 2009.
- [40] S. Ioffe and C. Szegedy, "Batch Normalization: Accelerating Deep Network Training by Reducing Internal Covariate Shift," in *Int. Conf. on Mach. Learn.* pmlr, Feb. 2015, pp. 448–456.
- [41] Y. Wu and K. He, "Group Normalization," *Int J Comput Vis*, vol. 128, no. 3, pp. 742–755, Mar. 2020.

APPENDIX A

HYPERPARAMETERS AND TRAINING DETAILS

We chose the third layer of the ResNet18 model as the cut layer. For the client models we replaced BatchNorm [40] layers with GroupNorm [41] layers. This is due to BatchNorm depending on the batch size and batch statistics, which is not compatible with frameworks such as PSL, where the local batch sizes can vary. GroupNorm has also shown to be more effective for non-IID data [41]. We chose a group size of 32 for all replaced GroupNorm layers. For FL and SFL we chose the the number of local epochs based on the number of clients K . We set the number of local epochs to $\log_2(K) - 1$ in all our experiments. As optimizer we used the mini-batch stochastic gradient descent algorithm with momentum. We chose a learning rate of 1×10^{-2} , a momentum of 0.9 and L_2 regularization with a weight decay of 5×10^{-4} . We used the cross entropy loss as our global loss function defined as:

$$L(\mathcal{B}^{(t)}; \mathbf{w}_s) = -\frac{1}{B} \sum_{i=1}^B \sum_{m=1}^M y_{i,m} \log(\hat{y}_{i,m})$$

$$\text{where } \hat{y}_i = f(f(\mathbf{x}_i; \mathbf{w}_c); \mathbf{w}_s)$$

For LDS we chose a convergence threshold of $\tau = 1 \times 10^{-5}$ and set $R = 0$ for all experiments. We always used the overall class labels of \mathcal{D}_0 as \mathbf{y} for the EM algorithm. All experiments were conducted on a workstation with an Intel Core i9-13900 CPU, 64 GB of DDR5 RAM and an NVIDIA GeForce A4000 GPU with 16 GB of VRAM. Appendix one text goes here. You can choose not to have a title for an appendix if you want by leaving the argument blank

APPENDIX B PROOFS

Proof of Lemma 1

We have $\mathbb{E}[Y_m] = B\beta_{0,m}$. It holds that $\mathbb{E}\left[\frac{Y_m}{B}\right] = \beta_{0,m}$ and $\text{Var}\left(\frac{Y_m}{B}\right) = \frac{1}{B^2} \text{Var}(Y_m)$. The Lemma follows from the Chebyshev inequality. \square

Proof of Lemma 2

According to the Markov inequality it holds that

$$\mathbb{P}\left(\left(\frac{Y'_m}{B} - \beta_{0,m}\right)^2 \geq \epsilon^2\right) \leq \frac{\mathbb{E}\left[(Y'_m - B\beta_{0,m})^2\right]}{B^2\epsilon^2}$$

$$\begin{aligned} \mathbb{E}\left[(Y'_m - B\beta_{0,m})^2\right] &= \mathbb{E}\left[(Y'_m - \mathbb{E}[Y'_m] + \mathbb{E}[Y'_m] - B\beta_{0,m})^2\right] \\ &= \mathbb{E}\left[(Y'_m - \mathbb{E}[Y'_m])^2\right] + 2(\mathbb{E}[Y'_m] - B\beta_{0,m})\mathbb{E}[Y'_m - \mathbb{E}[Y'_m]] \\ &\quad + (\mathbb{E}[Y'_m] - B\beta_{0,m})^2 \\ &= \text{Var}(Y'_m) + (\mathbb{E}[Y'_m] - \mathbb{E}[Y_m])^2 \end{aligned}$$

Where the last equality follows from $\mathbb{E}[Y'_m - \mathbb{E}[Y'_m]] = 0$ and $\mathbb{E}[Y_m] = B\beta_{0,m}$. Recognize that:

$$\left|\frac{Y'_m}{B} - \beta_{0,m}\right| \geq \epsilon \implies \left(\frac{Y'_m}{B} - \beta_{0,m}\right)^2 \geq \epsilon^2$$

Therefore, the bound is:

$$P\left(\left|\frac{Y'_m}{B} - \beta_{0,m}\right| \geq \epsilon\right) \leq \frac{\text{Var}(Y'_m) + (\mathbb{E}[Y'_m] - \mathbb{E}[Y_m])^2}{B^2\epsilon^2}$$

\square

Proof of Theorem 1

We first show that if either $\beta_{k,m} = \beta_{0,m}$ or $B_k = B\frac{D_k}{D}$ for all $k \in \mathcal{K}$ then $\mathbb{E}[Y'_m] = \mathbb{E}[Y_m]$ for all $m \in \mathcal{M}$.

Case 1: $\beta_{k,m} = \beta_{0,m}$.

$$\begin{aligned} \mathbb{E}[Y'_m] &= \sum_{k \in \mathcal{K}} B_k \beta_{k,m} = \sum_{k \in \mathcal{K}} B_k \beta_{0,m} = \beta_{0,m} \sum_{k \in \mathcal{K}} B_k \\ &= \beta_{0,m} B = \mathbb{E}[Y_m] \end{aligned}$$

Case 2: $B_k = B\frac{D_k}{D}$.

$$\begin{aligned} D\beta_{0,m} &= \sum_{k \in \mathcal{K}} D_k \beta_{k,m} \\ \iff B\beta_{0,m} &= \sum_{k \in \mathcal{K}} B\frac{D_k}{D} \beta_{k,m} = \sum_{k \in \mathcal{K}} B_k \beta_{k,m} \\ \iff \mathbb{E}[Y'_m] &= \mathbb{E}[Y_m] \end{aligned}$$

Consequently, the bias term in Lemma 2 is zero and it holds that:

$$P\left(\left|\frac{Y'_m}{B} - \beta_{0,m}\right| \geq \epsilon\right) \leq \frac{\text{Var}(Y'_m)}{B^2\epsilon^2}$$

We now show that $\text{Var}(Y'_m) \leq \text{Var}(Y_m)$ always holds. We have:

$$\begin{aligned} \text{Var}(Y_m) &= B\beta_{0,m}(1 - \beta_{0,m}) \\ &= B\left(\sum_{k \in \mathcal{K}} \frac{B_k}{B}\beta_{k,m}\right)\left(1 - \sum_{k \in \mathcal{K}} \frac{B_k}{B}\beta_{k,m}\right) \\ &\geq B\sum_{k \in \mathcal{K}} \frac{B_k}{B}\beta_{k,m}(1 - \beta_{k,m}) \\ &= \sum_{k \in \mathcal{K}} B_k\beta_{k,m}(1 - \beta_{k,m}) = \text{Var}(Y'_m) \end{aligned} \quad (6)$$

Where Equation (6) follows from Jensen's inequality with the concave function $\varphi(x) = x(1-x)$. Equality holds if and only if $\beta_{k,m} = \beta_{0,m}$ for all $k \in \mathcal{K}$. Thus, it holds that

$$\frac{\text{Var}(Y'_m)}{B^2\epsilon^2} \leq \frac{\text{Var}(Y_m)}{B^2\epsilon^2}$$

which completes the proof. \square

Proof of Corollary 1

$$\mathbb{E}[Y'_m] = \sum_{k=1}^K B\pi_k\beta_{k,m} = \sum_{k=1}^K B_k\beta_{k,m}$$

Where $B_k = B\pi_k = B\frac{D_k}{D}$. According to Theorem Theorem 1 the bound holds. \square

Proof of Proposition 1

We introduce a Lagrange multiplier λ to ensure the constraint $\sum_{k \in \mathcal{K}} \pi_k = 1$, which yields the following objective function:

$$\mathcal{L}(\boldsymbol{\pi}, \lambda) = \mathcal{Q}(\boldsymbol{\pi}, \boldsymbol{\pi}^{\text{old}}) + \ln p(\boldsymbol{\pi} \mid \boldsymbol{\alpha}) + \lambda \left(\sum_{k \in \mathcal{K}} \pi_k - 1 \right)$$

Taking the derivative with respect to π_k and setting it to zero, we get:

$$\begin{aligned} \frac{\partial \mathcal{L}(\boldsymbol{\pi}, \lambda)}{\partial \pi_k} &\stackrel{!}{=} 0 \\ \Leftrightarrow \sum_{n=1}^N \frac{\gamma_{n,k}}{\pi_k} + \frac{\alpha_k - 1}{\pi_k} + \lambda &= 0 \\ \Leftrightarrow \sum_{n=1}^N \gamma_{n,k} + \alpha_k - 1 + \lambda\pi_k &= 0 \\ \Leftrightarrow \sum_{k'=1}^K \sum_{n=1}^N \gamma_{n,k'} + \sum_{k'=1}^K (\alpha_{k'} - 1) + \sum_{k'=1}^K \lambda\pi_{k'} &= 0 \\ \Leftrightarrow N + \alpha_0 - K + \lambda \sum_{k=1}^K \pi_k &= 0 \\ \Leftrightarrow \lambda &= -N - \alpha_0 + K \end{aligned} \quad (7)$$

Inserting the result back into Equation (7) yields:

$$\begin{aligned} \sum_{n=1}^N \gamma_{n,k} + \alpha_k - 1 + \lambda\pi_k &= 0 \\ \Leftrightarrow N_k + \alpha_k - 1 &= (N + \alpha_0 - K)\pi_k \\ \Leftrightarrow \pi_k &= \frac{N_k + \alpha_k - 1}{N + \alpha_0 - K} \end{aligned}$$

\square